

July 22, 2008

Magnetic properties of GaMnAs nanodot arrays fabricated using porous alumina templates

S. P. Bennett

Northeastern University

L. Menon

Northeastern University

D. Heiman

Northeastern University

Recommended Citation

Bennett, S. P.; Menon, L.; and Heiman, D., "Magnetic properties of GaMnAs nanodot arrays fabricated using porous alumina templates" (2008). *Physics Faculty Publications*. Paper 531. <http://hdl.handle.net/2047/d20002679>

Magnetic properties of GaMnAs nanodot arrays fabricated using porous alumina templates

S. P. Bennett, L. Menon, and D. Heiman

Citation: *J. Appl. Phys.* **104**, 024309 (2008); doi: 10.1063/1.2955450

View online: <http://dx.doi.org/10.1063/1.2955450>

View Table of Contents: <http://jap.aip.org/resource/1/JAPIAU/v104/i2>

Published by the [American Institute of Physics](#).

Related Articles

Controllable aggregates of silver nanoparticle induced by methanol for surface-enhanced Raman scattering
Appl. Phys. Lett. **101**, 173109 (2012)

CdSe quantum dots-poly(3-hexylthiophene) nanocomposite sensors for selective chloroform vapor detection at room temperature
Appl. Phys. Lett. **101**, 173108 (2012)

An "edge to edge" jigsaw-puzzle two-dimensional vapor-phase transport growth of high-quality large-area wurtzite-type ZnO (0001) nanohexagons
Appl. Phys. Lett. **101**, 173105 (2012)

Ti-doped hematite nanostructures for solar water splitting with high efficiency
J. Appl. Phys. **112**, 084312 (2012)

Near-infrared enhanced carbon nanodots by thermally assisted growth
Appl. Phys. Lett. **101**, 163107 (2012)

Additional information on J. Appl. Phys.

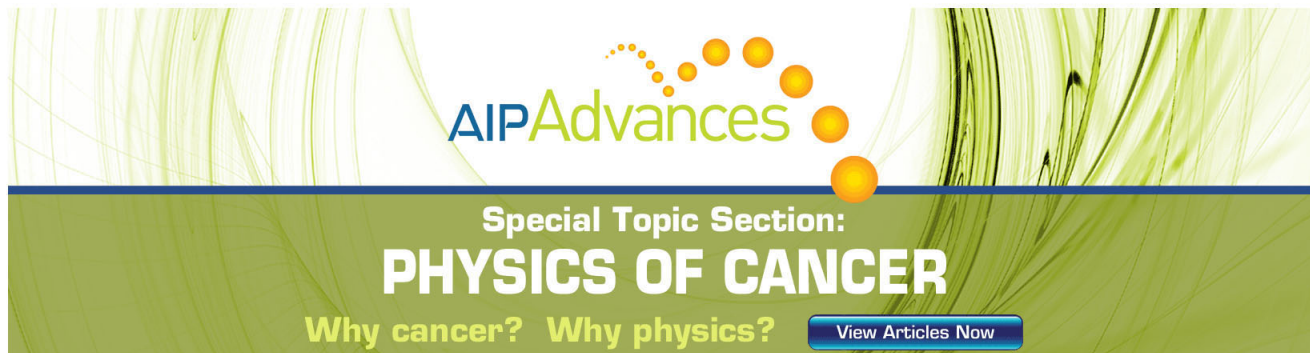
Journal Homepage: <http://jap.aip.org/>

Journal Information: http://jap.aip.org/about/about_the_journal

Top downloads: http://jap.aip.org/features/most_downloaded

Information for Authors: <http://jap.aip.org/authors>

ADVERTISEMENT



AIP Advances

Special Topic Section:
PHYSICS OF CANCER

Why cancer? Why physics? [View Articles Now](#)

Magnetic properties of GaMnAs nanodot arrays fabricated using porous alumina templates

S. P. Bennett, L. Menon, and D. Heiman^{a)}

Physics Department, Northeastern University, Boston, Massachusetts 02115, USA

(Received 11 March 2008; accepted 5 May 2008; published online 22 July 2008)

Ordered arrays of GaMnAs magnetic semiconductor nanodots have been fabricated using anodic porous alumina templates as etch masks. The magnetic behavior is studied for prepared arrays with 40 nm dot diameter, 15 nm dot thickness, and 80 nm periodicity. The disklike nanodots exhibit an easy axis for fields applied in the radial direction and a hard axis in the smaller direction. In the radial direction superparamagnetism is observed with a blocking temperature of 30 K. The fabrication technique is convenient for preparing nanodot arrays of compound semiconductors that cannot be formed by self-assembly techniques. © 2008 American Institute of Physics.

[DOI: [10.1063/1.2955450](https://doi.org/10.1063/1.2955450)]

INTRODUCTION

As research in nanoscale electronics and magnetics is flourishing, so is the demand for nanostructures of unique materials. Following the progress of growing two-dimensional (2D) epitaxial structures, there has been significant advancement in fabricating lower-dimensional structures, namely, nanodots, nanowires, and nanotubes. Fabrication of highly ordered nanodot arrays composed of quantum dot semiconductors¹ and ferromagnetic nanoparticles^{2,3} is drawing increased interest as advanced devices call for smaller nanostructured systems.^{1,4} Current research on the preparation of semiconducting nanodot arrays relies mainly on self-assembly during growth, such as InAs quantum dots in GaAs or postgrowth fabrication using photo lithography or electron beam lithography and etching. Another promising technique for fabricating nanodot arrays is the use of porous templates, such as anodic porous alumina. These can be used as shadow masks for direct deposition,⁵⁻⁷ selective etching,⁷⁻⁹ and preparation of imprint molds.^{10,11} There are several advantages of using these mask techniques: (1) the fabrication of smaller dot sizes <10 nm, (2) the rapid manufacture of large-size arrays, and (3) the possibility of fabricating nanodot arrays made from a larger class of materials, including metals, compound semiconductors, and insulators.

This report describes the fabrication and magnetic properties of GaMnAs magnetic semiconductor nanodot arrays. The fabrication process uses anodic porous alumina as deposition masks followed by plasma etching. A thin film of the ferromagnetic semiconductor GaMnAs is first deposited on a GaAs substrate. This is followed by the deposition of metal nanodots on the film surface using porous alumina as a mask. A key feature of this process is the long-range, room-temperature migration of the metal through the relatively long and thin nanochannels. The metal nanodots are then used to block the etching action of an argon plasma that removes the film material between the dots. The resulting

arrays of disklike GaMnAs nanodots had a dot diameter of 40 nm, thickness of 15 nm, and periodicity of 80 nm. The magnetic properties of the nanodots were investigated for various directions of the magnetic field and for field-cooled (FC) and zero-field-cooled (ZFC) conditions. When the magnetic field is applied in the plane of the disks, the ZFC magnetic moment has a maximum at a temperature of 30 K. This behavior is assigned to superparamagnetism with a blocking temperature of $T_B=30$ K. In contrast to this easy magnetic axis for fields applied on the plane of the dots, a hard magnetic axis is observed for fields applied perpendicular to the plane of the disks, where no thermal blocking mechanism is observed.

FABRICATION

A multistep process was used to fabricate the nanodot arrays using porous alumina masks. This process is similar to a technique used to fabricate arrays of Si nanodots.⁷ The porous alumina masks were fabricated using a dual anodization process on high-purity Al foil.¹² Anodization was carried out at a constant voltage of 40 V in a 3% oxalic acid solution. The Al foil was first anodized for 10–12 h. Since the bottom of the pores in this first layer of alumina has improved spatial ordering, it is removed using a mixture of chromic-phosphoric acid to leave a dimpled pattern on the Al surface that is highly ordered.¹³ Next, the patterned surface is reanodized for a short time in 3% oxalic acid to produce the desired ordered array of pores. The top surface of the film is then protected against etching by coating it with an organic layer (GE-7031 varnish), after which the bottom Al layer is removed using a saturated HgCl₂ solution. The barrier layer of alumina below the porous layer is removed using 5 wt % phosphoric acid for about 80 min. The masks typically had pore diameters of ~40 nm, pore spacing of 80 nm, and mask thickness of ~400–800 nm. The scanning electron microscope (SEM) micrographs of these templates were taken using a Hitachi S-4800 field-emission SEM. The SEM micrographs confirmed that the pores extend all the way through the mask and are open at both ends.

^{a)}Electronic mail: heiman@neu.edu.

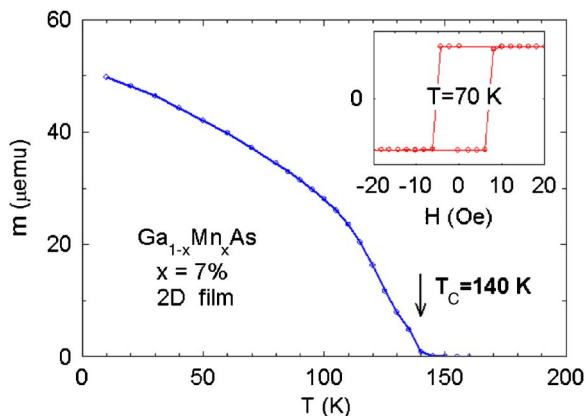


FIG. 1. (Color online) Magnetic moment vs temperature for a ferromagnetic 2D film of $\text{Ga}_{1-x}\text{Mn}_x\text{As}$ and $x=0.07$ in an applied magnetic field of 5 Oe. The moment drops to zero at the ferromagnetic Curie temperature, $T_C=140$ K. The inset shows the ferromagnetic hysteresis at $T=70$ K.

The nanodot arrays of GaMnAs were fabricated using the following procedure: First, a 10 nm thick buffer layer of GaAs was grown on an oxide-desorbed, semi-insulating GaAs substrate at a temperature of 580 °C using a molecular beam epitaxy (MBE). This was followed by the epitaxial growth of a 15 nm thick $\text{Ga}_{1-x}\text{Mn}_x\text{As}$, $x=7\%$ layer at a substrate temperature of 255 °C. The sample was then annealed^{14,15} in air at 230 °C for 20 min to increase its ferromagnetic Curie temperature. Magnetic measurements were carried out using a superconducting quantum interference device magnetometer (Quantum Design MPMS XL-5). Figure 1 shows the magnetic moment of the GaMnAs 2D film as a function of the temperature in the range of $T=10\text{--}200$ K. It can be seen that the magnetic moment collapses to zero at the ferromagnetic transition temperature of $T_C=140$ K. The inset shows the hysteresis at $T=70$ K with a coercive field $H_C=6$ Oe.

The porous alumina masks were placed on the top surface of the GaMnAs. Figure 2(a) shows a section of the porous alumina mask. Cr metal was then deposited through the pores in the mask via thermal evaporation. The Cr was chosen because it has a much slower etch rate than the underlying GaMnAs layer. The Cr was deposited at a rate of ~ 0.1 nm/sec to an equivalent thickness of 35–40 nm in a vacuum of 7×10^{-7} torr. In spite of the relatively high aspect ratio of the pores, with length/diameter of $\sim 10\text{--}20$, the metal has sufficient mobility at room temperature to deposit a significant amount of material onto the film surface. The mask was then dissolved using a 5% phosphoric acid solution. This resulted in Cr nanodot arrays on the surface of the GaMnAs film, where they act as masks in the next etching step. Lastly, a plasma etch process was used to remove the unwanted GaMnAs film layer surrounding the Cr nanodots. For this step, a reactive ion etcher (South Bay Technology RIE 2000) was used with high-purity argon gas as the etchant. The etching time was adjusted so that it was sufficient to remove the GaMnAs film between the metal nanodots, but not long enough to completely remove the Cr nanodots. The appropriate etching times were several hours at an argon pressure of 100 mtorr.

Figure 2(b) shows a portion of the edge of the sample,

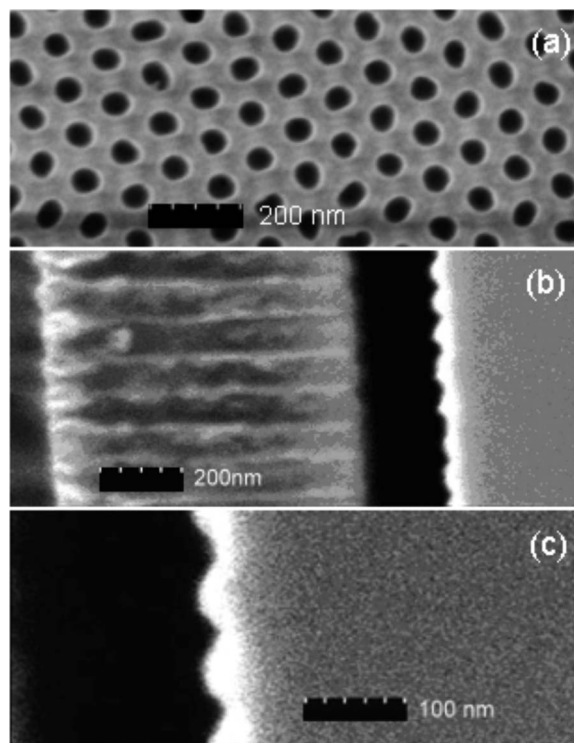


FIG. 2. SEM micrographs. Those shown are (a) anodic porous alumina mask, (b) cross section of the porous alumina mask lifted away from the substrate (left) and the Cr nanodots that were deposited on the substrate through the pores (right), and (c) side view of the GaMnAs/Cr nanodots after plasma etching.

where the mask was pulled away from the surface of the sample. In this image the Cr dots are seen on the right side and the cross section of the mask is on the left side. Notice that the dots are aligned next to their associated pores. The heights of the deposited Cr dots are approximately 35 nm, somewhat less than the 40–45 nm thickness of the Cr layer that was deposited on top of the mask. The brighter material seen on the left side of the mask (top of the pores) is the residual Cr. This buildup eventually impeded the flow of the Cr through the mask to the substrate. After the masks were removed, the Cr dots remained on the surface of the layered substrate and provided masking during the plasma etching. The resulting array of the GaMnAs nanodots has the same triangular symmetry and spacing as the pores in the alumina mask. The diameter of the bumps is 35–40 nm, approximately the same as that of the pores in the mask. Figure 2(c) shows the nanodots in cross section, revealing dot heights in the range of 30–35 nm.

RESULTS

Figure 3 shows the magnetic properties of a GaMnAs nanodot array for fields applied on the plane of the disklike nanodots. The magnetic moment is plotted as a function of temperature $m(T)$ for ZFC and FC conditions. In each case, the sample was cooled from room temperature to $T=5$ K, either in an applied field of $H=100$ Oe (FC) or cooled in zero magnetic field (ZFC). After reaching the low temperature, a small field of $H=100$ Oe was applied and the magnetic moment was measured as a function of the increasing

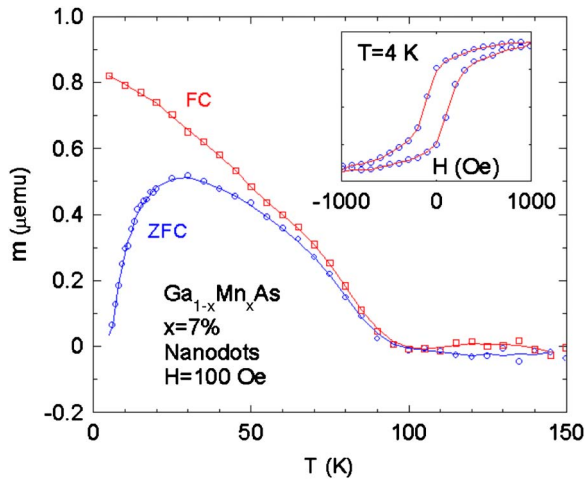


FIG. 3. (Color online) Magnetic moment vs temperature of a GaMnAs nanodot array in an applied field of $H=100$ Oe. The FC and ZFC data are shown, revealing superparamagnetic behavior with a blocking temperature of $T_B=30$ K. The inset shows the ferromagnetic hysteresis at $T=4$ K.

temperature. While the curves are equivalent in temperatures above $T=60$ K, there is a significant difference in the ZFC and FC conditions seen below $T=60$ K. Below this temperature the ZFC moment is significantly smaller than the FC moment. This behavior is assigned to superparamagnetism—a consequence of the small magnetic moment of nanometer size ferromagnetic particles and signature of reduced dimensions.^{16,17} At low temperature, $T < 30$ K, the ZFC moment increases in increasing temperature because the direction of the moments in the magnetic nanodots, which were originally frozen in random orientations during the ZFC process, requires increased thermal energy to become aligned with the small measuring field. The maximum in the ZFC moment is identified with the blocking temperature, $T_B=30$ K. This blocking temperature separates the paramagnetic behavior of $T > T_B$ and the ferromagnetic behavior of $T < T_B$. Below T_B the nanodots are ferromagnetic and magnetic hysteresis is observed, as shown in the inset of Fig. 3. At $T=4$ K, the magnetization saturates at a field of $H_S \sim 1000$ Oe and the hysteresis has a coercive field of $H_C=130$ Oe. The ZFC curve is relatively broad and the broadening is attributed to nonuniformity in dot size and/or shape over the millimeter square dimension of the array.

Magnetic measurements were made for various directions of the applied magnetic field. An easy axis behavior was observed for fields applied in the plane of the disklike nanodots, while a hard axis was found for fields applied perpendicular to the disk plane. For the present arrays, the fabrication technique makes the plane of the disks lie parallel to the plane of the initial 2D epitaxial layer, the (001) plane. The same easy/hard axis behavior is found for 2D films of GaMnAs. This is attributed to the strong biaxial crystalline anisotropy of the strained GaMnAs epitaxial layer on the slightly lattice mismatched GaAs substrate, rather than the shape anisotropy, which is several orders of magnitude weaker.¹⁸ Thus, the GaMnAs lattice in the nanodots is not appreciably relaxed and remains strongly affected by the strain of the lattice mismatch with the GaAs substrate. For fields applied in the plane of the disklike nanodots, no dis-

cernable difference was observed in the [110] and [1-10] crystalline directions. This is unlike that found in 2D layers of GaMnAs that exhibit uniaxial magnetic anisotropy for fields applied in the plane of the layers.¹⁹ This uniaxial anisotropy has been found to be dependent on the temperature, Mn concentration, and annealing conditions.²⁰ The in-plane easy axis shifts by 90° upon annealing due to an increase in the hole concentration and consequent increase in the saturation moment. This shift in the easy axis is a consequence of the relative magnitudes of the biaxial (K_C) and uniaxial (K_U) anisotropy constants. These change differently with temperature as they are proportional to the saturation moment with different power laws, where $K_C \propto m^4$ and $K_U \propto m^2$.²¹ For the nanodots it appears that the uniaxial anisotropy may be much smaller than the cubic anisotropy in the temperature region of interest. An effective anisotropy constant (K_E) for the nanodots can be deduced from the blocking temperature, where the ratio of anisotropy energy to thermal energy is given by $K_1 V/k_B T_B=25$ and $V=\pi D^2 H/4$. For the dot diameter $D=40$ nm, height $H=15$ nm, and $T_B=30$ K, $K_1 \sim 6000$ ergs/cm³. This is on the order of that found in a 2D epitaxial layer.²¹

CONCLUSION

Fabricating GaMnAs nanodots with the porous alumina as an etch mask is an example of nanofabrication of a semiconductor material, which is difficult to grow in nanoscale dimensions. The direct MBE growth of GaMnAs nanodots through a porous alumina deposition mask has not been successful²² in spite of the successful growth of GaAs and AlGaAs nanodots using a deposition mask.^{23,24} This is attributed to the required low growth temperature of GaMnAs (Ref. 25) at ~ 250 °C, which is evidently too low to allow the Mn to migrate through the pores. This mobility deficiency is essential to the growth of homogeneous 2D layers of GaMnAs, where the Mn mobility must be low enough to inhibit the Mn from clustering into self-assembled MnAs nanodots.

In conclusion, highly organized arrays of GaMnAs magnetic semiconductor nanodots have been fabricated using a porous alumina template-based process. The resulting 40 nm diameter nanodots were found to be superparamagnetic with a blocking temperature of $T_B=30$ K. This method can be applied to other semiconductor materials and heterostructures that cannot be fabricated using traditional methods of self-assembly. Heterostructures fabricated from metal and semiconductor layers can naturally lead to nanometer size electronic devices and device arrays for electronic circuits.

ACKNOWLEDGMENTS

This work was supported by NSF (Grant Nos. DMR-0305360 and ECCS-0551468).

¹R. Hanson, L. P. Kouwenhoven, J. R. Petta, S. Tarucha, and L. M. K. Vandersypen, *Rev. Mod. Phys.* **79**, 1217 (2007); see also arXiv:cond-mat/0610433.

²R. P. Cowburn, J. Magn. Magn. Mater. **242–245**, 505 (2002).

³M. A. Willard, L. Kurihara, E. E. Carpenter, S. Calvin, and V. G. Harris, *Int. Mater. Rev.* **49**, 125 (2004); *Encyclopedia of Nanoscience and Nano-*

- technology* (American Scientific, Stevenson Ranch, CA, 2004), Vol. 1, pp. 815–848.
- ⁴B. D. Terris and T. Thomson, *J. Phys. D* **38**, R199 (2005).
- ⁵H. Masuda, K. Yasui, and K. Nishio, *Adv. Mater. (Weinheim, Ger.)* **12**, 1031 (2000).
- ⁶C.-P. Li, I. V. Roshchin, X. Battle, M. Viret, F. Ott, and I. K. Schuller, *J. Appl. Phys.* **100**, 074318 (2006).
- ⁷J. Liang, H. Chik, A. Yin, and J. Xu, *J. Appl. Phys.* **91**, 2544 (2002).
- ⁸H. Masuda, M. Wantanabe, K. Yasui, D. Tryk, T. Rao, and A. Fujishima, *Adv. Mater. (Weinheim, Ger.)* **12**, 444 (2000).
- ⁹H. Hu and D. He, *Mater. Lett.* **60**, 1019 (2006).
- ¹⁰K. Yasui, K. Nishio, H. Nunokawa, and H. Masuda, *J. Vac. Sci. Technol. B* **23**, L9 (2005).
- ¹¹H. Masuda and K. Fukuda, *Science* **268**, 1466 (1995); H. Masuda, H. Yamada, M. Satoh, H. Asoh, M. Nakao, and T. Tamamura, *Appl. Phys. Lett.* **71**, 2770 (1997).
- ¹²O. Jessensky, F. Muller, and U. Gosele, *Appl. Phys. Lett.* **72**, 1173 (1998).
- ¹³L. E. Rehn, B. J. Kestel, P. M. Baldo, J. Hiller, A. W. McCormick, and R. C. Birtcher, *Nucl. Instrum. Methods Phys. Res. B* **206**, 490 (2003).
- ¹⁴K. C. Ku, S. J. Potashnik, R. F. Wang, S. H. Chun, P. Schiffer, N. Samarth, M. J. Seong, A. Mascarenhas, E. Johnston-Halperin, R. C. Myers, A. C. Gossard, and D. D. Awschalom, *Appl. Phys. Lett.* **82**, 2302 (2003).
- ¹⁵K. Edmonds, P. Boguslawski, K. Wang, R. Champion, S. Novikov, N. Farley, B. Gallagher, C. Foxon, M. Sawicki, T. Dietl, M. Nardelli, and J. Bernholc, *Phys. Rev. Lett.* **92**, 037201 (2004).
- ¹⁶E. C. Stoner and E. P. Wohlfarth, *Philos. Trans. R. Soc. London, Ser. A* **240**, 599 (1948); *IEEE Trans. Magn.* **27**, 3475 (1991).
- ¹⁷A. Aharoni, *Introduction to the Theory of Ferromagnetism* (Oxford Science, New York, 2000).
- ¹⁸C. Gould, K. Pappert, G. Schmidt, and L. W. Molenkamp, *Adv. Mater. (Weinheim, Ger.)* **19**, 323 (2007).
- ¹⁹U. Welp, V. K. Vlasko-Vlasov, A. Menzel, H. D. You, X. Liu, J. K. Furdyna, and T. Wojtowicz, *Appl. Phys. Lett.* **85**, 260 (2004).
- ²⁰M. Sawicki, K.-Y. Wang, K. W. Edmonds, R. P. Champion, C. R. Staddon, N. R. S. Farley, C. T. Foxon, E. Papis, E. Kamioska, A. Piotrowska, T. Dietl, and B. L. Gallagher, *Phys. Rev. B* **71**, 121302 (2005).
- ²¹K.-Y. Wang, M. Sawicki, K. W. Edmonds, R. P. Champion, S. Maat, C. T. Foxon, B. L. Gallagher, and T. Dietl, *Phys. Rev. Lett.* **95**, 217204 (2005).
- ²²S. P. Bennett, L. Zhang, Z. Wu, L. Menon, and D. Heiman (unpublished).
- ²³X. Mei, D. Kim, H. E. Ruda, and Q. X. Guo, *Appl. Phys. Lett.* **81**, 361 (2002).
- ²⁴X. Mei, M. Blumin, M. Sun, D. Kim, Z. H. Wu, H. E. Ruda, and Q. X. Guo, *Appl. Phys. Lett.* **82**, 967 (2003).
- ²⁵H. Ohno, *Science* **281**, 951 (1998).